

## Formation of accreting millisecond X-ray pulsars

Xiang He<sup>1,2,3</sup>, Xiang-Cun Meng<sup>1,2</sup> and Hai-Liang Chen<sup>1,2</sup>

<sup>1</sup> Yunnan Observatories, Chinese Academy of Sciences, Kunming 650216, China; [hexiang@ynao.ac.cn](mailto:hexiang@ynao.ac.cn)

<sup>2</sup> Key Laboratory for the Structure and Evolution of Celestial Objects, Chinese Academy of Sciences, Kunming 650216, China

<sup>3</sup> University of Chinese Academy of Sciences, Beijing 100049, China

Received 2018 September 11; accepted 2018 December 26

**Abstract** Accreting millisecond X-ray pulsars (AMXPs) are an important subclass of low-mass X-ray binaries (LMXBs), in which coherent millisecond X-ray pulsations can be observed during outburst states. They have dual characteristics of LMXBs and millisecond pulsars, providing a direct confirmation for the recycling scenario. However, their formation is not well understood. In this work, we simulate the evolution of LMXBs with the MESA code to explore the formation and evolution of AMXPs. Based on the binary evolutionary model of LMXBs and the model of accretion disk instability, we find that most of the observed AMXPs can be produced from LMXBs with orbital periods at the onset of Roche lobe overflow close to the bifurcation period and their observed properties can be explained by our models. The AMXPs with main sequence (MS) donors ultimately evolve into AMXPs with extremely low-mass He white dwarf donors. Moreover, our results indicate that these AMXPs with MS donors are likely to have donor stars near the terminal-age main sequence.

**Key words:** binaries: close — stars: evolution — stars: neutron — X-ray: binaries

### 1 INTRODUCTION

During the last two decades, since the first accreting millisecond X-ray pulsar (AMXP), SAX J1808.4–3658, was discovered in 1998 (Wijnands & van der Klis 1998), the number of AMXPs has increased to 22. AMXPs are a subclass of low-mass X-ray binaries (LMXBs) and coherent millisecond X-ray pulsations are detected during their outburst states (see Patruno & Watts 2012 and Campana & Di Salvo 2018 for reviews). Different from radio millisecond pulsars, AMXPs are in essence accretion-powered X-ray pulsars with weak magnetic fields ( $B \sim 10^8 - 10^9$  G) and short spin periods ( $P_s < 10$  ms) (Walter & Ferrigno 2017). It is widely accepted that binary millisecond pulsars are produced from the evolution of LMXBs (i.e., the recycling scenario, Alpar et al. 1982; Radhakrishnan & Srinivasan 1982). In this scenario, accretion onto a neutron star (NS) not only spins up the NS but also leads to the decay of its magnetic field. If an NS is fully recycled, it will become a millisecond pulsar. The discovery of the first AMXP provides a direct confirmation for the recycling scenario. Moreover, AMXPs are also important for the studies of ac-

cretion physics of compact binaries and physical properties of NSs (e.g., Poutanen & Gierliński 2003; Watts 2012).

So far, most of the observed AMXPs are faint X-ray transients whose outbursts typically last for weeks to months with peak X-ray luminosities of  $10^{36} - 10^{37}$  erg s<sup>-1</sup> (e.g., Archibald et al. 2015; Wu et al. 2010). Meanwhile, there are three (quasi-)persistent X-ray sources whose outbursts last for years rather than weeks to months, i.e., HETE J1900.1–2455 (Degenaar et al. 2017), IGR J17602–6143 (Strohmayer & Keek 2017) and MAXI J0911–655 (Bult 2017). The persistent and transient behaviors of LMXBs are suggested to originate from the thermal-ionization disk instability (see Lasota 2001 for a review). In a typical transient LMXB, the NS mainly stores material in the disk lasting for months to years with an X-ray luminosity of  $10^{31} - 10^{33}$  erg s<sup>-1</sup> during a quiescent state. During an outburst state, the NS accretes material from the disk suddenly lasting for days to weeks with a peak X-ray luminosity of  $10^{36} - 10^{38}$  erg s<sup>-1</sup>. However, the two AMXPs, i.e., PSR J1023+0038 (Papitto et al. 2014) and XSS J12270–4859 (Papitto et al. 2015), are very faint

**Table 1** List of Observed Properties of 22 AMXPs

	Source Name	$P_s$ (Hz)	$P_{\text{orb}}$ (h)	$M_d$ ( $M_\odot$ )	Donor type MS/BD/WD	$L_X^{\text{peak}}$ ( $10^{36} \text{ erg s}^{-1}$ )	Ref.
1	SAX J1808.4–3658	401	2.01	0.044	BD	3.9	[1],[2]
2	HETE J1900.1–2455	377	1.39	0.016	BD	4.9	[3]
3	IGR J00291+5934	599	2.46	0.040	BD	9.7	[4]
4	IGR J17379–3747	468	1.88	0.012	BD	0.9	[5]
5	SAX J1748.9–2021	442	8.77	0.106	MS	47.0	[6]
6	IGR J17511–3057	245	3.47	0.142	MS	7.2	[7]
7	XTE J1814–338	314	4.27	0.176	MS	4.4	[8]
8	IGR J17498–2921	401	3.84	0.176	MS	11.3	[9]
9	IGR J18245–2452	254	11.03	0.185	MS	8.0	[10]
10	IGR J17591–2342	527	8.80	0.374	MS	6.1	[11]
11	Aql X-1	550	18.95	0.60	MS	87.4	[12]
12	XSS J12270–4859	593	6.91	0.36	MS	0.13	[13]
13	Swift J1749.4–2807	518	8.82	0.631	MS	5.2	[14]
14	PSR J1023+0038	592	4.75	0.142	MS	0.14	[15]
15	XTE J1751–305	435	0.71	0.014	WD	15.0	[16]
16	XTE J0929–314	185	0.73	0.008	WD	4.4	[17]
17	XTE J807–294	190	0.67	0.007	WD	8.2	[18]
18	NGC 6440 X-2	206	0.95	0.007	WD	2.6	[19]
19	Swift J1756.9–2508	182	0.91	0.007	WD	6.3	[20]
20	MAXI J0911–655	340	0.74	0.024	WD	4.7	[21]
21	IGR J17602–6143	164	0.63	0.006	WD	0.8	[22]
22	IGR J16597–3704	105	0.77	0.006	WD	6.5	[23]

Notes: [1] Wijnands & van der Klis (1998); [2] Hartman et al. (2008); [3] Kaaret et al. (2006); [4] Markwardt et al. (2004); [5] Sanna et al. (2018c); [6] Patruno et al. (2009); [7] Markwardt et al. (2009); [8] Krauss et al. (2005); [9] Papitto et al. (2011); [10] Papitto et al. (2013); [11] Sanna et al. (2018b); [12] Casella et al. (2008); [13] Papitto et al. (2015); [14] Altamirano et al. (2010a); [15] Archibald et al. (2009); [16] Markwardt et al. (2002); [17] Galloway et al. (2002); [18] Falanga et al. (2005); [19] Altamirano et al. (2010b); [20] Krimm et al. (2007); [21] Sanna et al. (2017); [22] Strohmayer et al. (2018); [23] Sanna et al. (2018a).

X-ray transients (VFXTs) with X-ray luminosities of  $\sim 10^{34} \text{ erg s}^{-1}$  (Wijnands et al. 2006). From the disk instability model (DIM), we expect that most AMXPs would be observed as radio pulsars in quiescent states where the radio emission is rotation-powered and as X-ray pulsars in outburst states where the X-ray emission is accretion-powered. However, only three transitional AMXPs, i.e., PSR J1023+0038, IGR J18245–2452 and XSS J12270–4859, show transitions between rotation-powered states and accretion-powered states (see Papitto 2016 for details). Furthermore, these transitional AMXPs are observed as redback pulsars during quiescent states, which may suggest that the high energy emission from pulsars is ablating their companions similar to eclipsing binary millisecond pulsars (e.g., Roberts 2013; Chen et al. 2013; Benvenuto et al. 2014; Jia & Li 2015). Given that a small part of AMXPs behave as redback pulsars, the evaporation by the pulsar may not be important for the formation of most AMXPs.

According to the distribution of orbital periods ( $P_{\text{orb}}$ ) and donor types, these observed AMXPs can be roughly divided into three groups:  $P_{\text{orb}} < 1 \text{ h}$ ,  $1 \text{ h} < P_{\text{orb}} < 3 \text{ h}$

and  $3 \text{ h} < P_{\text{orb}} < 19 \text{ h}$ . Eight AMXPs with  $P_{\text{orb}} < 1 \text{ h}$  are ultra-compact X-ray binaries (UCXBs) and their donor stars are extremely low-mass He/CO white dwarfs (WDs). Four AMXPs with  $1 \text{ h} < P_{\text{orb}} < 3 \text{ h}$ , i.e., SAX J1808.4–3658, HETE J1900.1–2455, IGR J17379–3747 and IGR J00291+5934, possess brown dwarf (BD) donors. The rest of the AMXPs with  $3 \text{ h} < P_{\text{orb}} < 19 \text{ h}$  have main sequence (MS) donors. For these AMXPs with relatively short orbital periods ( $P_{\text{orb}} < 1 \text{ d}$ ), Deloye (2008) suggested that their formation can be associated with the evolution of CV-like LMXBs and UCXBs. From the point of view of binary evolution, there exists a critical orbital period at the onset of Roche lobe overflow (RLOF), defined as the bifurcation period ( $P_{\text{orb}}^{\text{bif}}$ ), which separates the formation of diverging systems from that of converging systems (Pylyser & Savonije 1988, 1989). Generally, if the orbital period at the onset of RLOF ( $P_{\text{orb}}^{\text{RLOF}}$ ) is less than  $P_{\text{orb}}^{\text{bif}}$ , the orbital period will decrease and converging systems, i.e. CV-like LMXBs and UCXBs, will be produced. Otherwise, the orbital period will increase and diverging LMXBs are formed. More precisely, if the MS donor is relatively unevolved at the onset of RLOF, the evolution has

similar evolutionary characteristics to that of a cataclysmic variable (so-called CV-like LMXB) and the donor star will ultimately become a brown dwarf (e.g., Podsiadlowski et al. 2002; Lin et al. 2011). If the central hydrogen of the MS donor is almost exhausted at the beginning of RLOF, the binary will evolve into a UCXB and an AMXP with an extremely low-mass He WD is likely to be formed (e.g., Podsiadlowski et al. 2002; Nelson & Rappaport 2003). This formation channel needs finely tuned initial parameters, thus some mechanisms are put forward to improve it (e.g., Ma & Li 2009; Chen & Podsiadlowski 2016). It is worth noting that an initial NS+MS binary can first evolve into a detached MSP+He WD binary with a compact orbit ( $P_{\text{orb}} \simeq 2\text{--}9$  h) if  $P_{\text{orb}}^{\text{RLOF}}$  is very close to  $P_{\text{orb}}^{\text{bif}}$  (e.g., Jia & Li 2014; Istrate et al. 2014). Then the He WD fills its Roche lobe and the binary finally evolves into a UCXB (e.g., Sengar et al. 2017). Apart from being formed from the evolved MS channel, AMXPs in UCXBs can also be produced via the WD channel (Rasio et al. 2000; Yungelson et al. 2002) and the helium star channel (Yungelson 2008). The latter two scenarios generally occur after an intermediate-mass X-ray binary experiences a common-envelope phase. However, recent hydrodynamic simulation shows that only NS+WD systems with He WD masses less than  $0.2 M_{\odot}$  can evolve into UCXBs with He-rich donors (Bobrick et al. 2017). Therefore, Bobrick et al. (2017) concluded that the two AMXPs with CO WDs, i.e., XTE J0929–314 and XTE J807–294, can only be produced from the NS+He star channel. If the donor star starts mass transfer at its (sub-)giant branch for an initial NS+MS binary, the system will evolve into a diverging LMXB and ultimately become a detached MSP+He WD system with  $P_{\text{orb}} > 1$  d (e.g., Tauris & Savonije 1999; Shao & Li 2012). To date, no AMXP is found in diverging LMXBs with  $P_{\text{orb}} > 1$  d. It may be related to the short evolutionary timescales of diverging LMXBs (Shao & Li 2015) or the magnetic field screening caused by a high accretion rate (Cumming et al. 2001). In a word, the evolution of LMXBs might explain the formation of most AMXPs via stable mass transfer.

In this paper, in order to study the formation and evolution of AMXPs, we model the evolution of LMXBs with a stellar evolution code. In view of the DIM, we want to examine whether LMXBs can explain the observed properties (e.g., orbital period, donor mass and persistent and transient behaviors) of most AMXPs and whether there exist evolutionary connections among AMXPs with different types of donors. In particular, we also investigate and diagnose their donor types in our models. This paper is structured as follows. In Section 2, we present the meth-

ods and assumptions in our calculations. In Section 3, we compare the results of our models with the observed properties of AMXPs. Finally, a brief discussion is presented in Section 4 and the main conclusions are given in Section 5.

## 2 NUMERICAL METHODS AND PHYSICAL ASSUMPTIONS

We use the stellar evolution code, Modules for Experiments in Stellar Astrophysics (MESA, version 8845, Paxton et al. 2011, 2013, 2015, 2018) to simulate the evolution of LMXBs. The binary orbit is assumed to be circular and the initial system consists of an NS and a zero-age main sequence (ZAMS) star with the solar chemical composition ( $X = 0.70$ ,  $Y = 0.28$  and  $Z = 0.02$ ). The NS is treated as a point mass and its initial mass is assumed to be  $1.4 M_{\odot}$ . The initial donor masses ( $M_{\text{d}}^{\text{i}}$ ) are  $1.0 M_{\odot}$  and  $1.3 M_{\odot}$ . We have tested that binary systems with initial donor masses ranging from  $1.0 M_{\odot}$  to  $2.0 M_{\odot}$  can also produce similar results, which are not shown in the following. We stop the calculation when the evolutionary time reaches 13.7 Gyr or the donor mass is smaller than  $0.005 M_{\odot}$  at which point the donor star is likely to be tidally disrupted (Ruderman & Shaham 1985; Sengar et al. 2017).

### 2.1 Disk Instability Model

During the evolution of an LMXB, if the donor star fills its Roche lobe, it starts to transfer material to the NS and the material will form a disk around the NS. Then the NS accretes material from the disk and the system appears as an LMXB with the release of the gravitational potential energy of the accreted material. Generally, the LMXB may appear as either a persistent or transient X-ray source, depending on whether the accretion disk is stable or not (e.g., van Paradijs 1996; Dubus et al. 1999; Lasota 2001). When the mass-transfer rate falls below a critical mass-transfer rate, the accretion disk will experience a thermal-viscous instability, and the LMXB becomes a transient source which will go through a short-lived outburst phase and a long-term quiescent phase. The duty cycle ( $d$ ) is estimated by  $d = t_{\text{out}}/t_{\text{rec}}$ , where  $t_{\text{out}}$  and  $t_{\text{rec}}$  are the outburst duration and the recurrence period, respectively. For typical transient X-ray sources,  $d$  is  $\sim 0.1\text{--}0.01$  (e.g., Williams et al. 2006; Yan & Yu 2015). When the mass-transfer rate is larger than the critical mass-transfer rate, the accretion disk is always stable, and the LMXB becomes a persistent source. The critical mass-transfer rate is mainly determined by the thermal-ionization instability of the disk. In addition, the observed persistent X-ray

sources show that irradiation heating of the disk is not negligible (e.g., van Paradijs 1996; Coriat et al. 2012). Here,

we adopt the critical mass-transfer rate ( $\dot{M}_{\text{cr}}$ ) under an irradiated solar-composition disk (Lasota et al. 2008),

$$\dot{M}_{\text{cr}} = 9.5 \times 10^{14} C_{-3}^{-0.36} \alpha_{0.1}^{0.04+0.01 \log C_{-3}} R_{10}^{2.39-0.10 \log C_{-3}} M_{\text{NS}}^{-0.64+0.08 \log C_{-3}} \text{ g s}^{-1}, \quad (1)$$

where  $C = 10^{-3} C_{-3}$ ,  $\alpha = 0.1 \alpha_{0.1}$ ,  $R = 10^{10} R_{10}$  cm and  $M_{\text{NS}}$  are the irradiation parameter, the viscosity parameter, the outer radius of the accretion disk and the NS mass, respectively. Based on a fundamental test of the DIM, a simple and reasonable formula is given by Coriat et al. (2012),

$$\dot{M}_{\text{cr}} = 2.9 \times 10^{15} \left( \frac{P_{\text{orb}}}{1 \text{ h}} \right)^{1.59} \text{ g s}^{-1}, \quad (2)$$

where  $P_{\text{orb}}$  is the binary orbital period in units of hour.

## 2.2 Mass and Orbital Angular Momentum Loss

In our calculations, three different mechanisms are involved in the evolution of orbital angular momentum, i.e. gravitational wave radiation (GR), magnetic braking (MB) and mass loss (ML). So the total orbital angular momentum loss ( $\dot{J}_{\text{orb}}$ ) is

$$\dot{J}_{\text{orb}} = \dot{J}_{\text{GR}} + \dot{J}_{\text{MB}} + \dot{J}_{\text{ML}}, \quad (3)$$

where  $\dot{J}_{\text{GR}}$ ,  $\dot{J}_{\text{MB}}$  and  $\dot{J}_{\text{ML}}$  represent the corresponding orbital angular momentum loss due to GR, MB and ML, respectively.  $\dot{J}_{\text{MB}}$  is adopted from Rappaport et al. (1983),

$$\dot{J}_{\text{MB}} = -6.82 \times 10^{34} \left( \frac{M_{\text{d}}}{1.0 M_{\odot}} \right) \left( \frac{R_{\text{d}}}{R_{\odot}} \right)^4 \left( \frac{1 \text{ d}}{P_{\text{orb}}} \right)^3 [\text{dyn cm}], \quad (4)$$

where  $R_{\text{d}}$  is the donor radius in units of  $R_{\odot}$ ,  $M_{\text{d}}$  is the donor mass in units of  $M_{\odot}$  and  $P_{\text{orb}}$  is the binary orbital period in units of days. When the donor star becomes fully convective, the magnetic braking is assumed to be turned off.

$\dot{J}_{\text{GR}}$  is given by Landau & Lifshitz (1971),

$$\dot{J}_{\text{GR}} = -\frac{32}{5c^5} \left( \frac{2\pi G}{P_{\text{orb}}} \right)^{7/3} \frac{(M_{\text{NS}} M_{\text{d}})^2}{(M_{\text{NS}} + M_{\text{d}})^{2/3}}, \quad (5)$$

where  $G$  and  $c$  are the gravitational constant and the light speed, respectively.

Following Tauris & Savonije (1999) and Tauris et al. (2013), we assume that only 30% of the transferred material is retained by the NS. The rest is lost via an isotropic wind and carries away the specific orbital angular momentum of the NS. Regarding the accretion during a transient LMXB, the accretion rate of the NS during an outburst state may be limited to the Eddington accretion rate ( $\dot{M}_{\text{Edd}}$ ) (e.g., Chen & Panei 2011; Liu & Chen 2011). Thus, the averaged accretion rate of the NS ( $\dot{M}_{\text{NS}}^{\text{av}}$ ) is roughly given by

$$\dot{M}_{\text{NS}}^{\text{av}} = \begin{cases} \beta \cdot \min(|\dot{M}_{\text{tr}}|, \dot{M}_{\text{Edd}}), & \dot{M}_{\text{tr}} \geq \dot{M}_{\text{cr}} \\ \beta \cdot \min(|\dot{M}_{\text{tr}}|, \dot{M}_{\text{Edd}} \cdot d), & \dot{M}_{\text{tr}} < \dot{M}_{\text{cr}}, \end{cases} \quad (6)$$

where the mass-transfer rate ( $\dot{M}_{\text{tr}}$ ) is computed according to the prescription of Ritter (1988), and the accretion efficiency of the NS ( $\beta$ ) and the duty cycle ( $d$ ) are taken to be 0.3 and 0.01, respectively. The corresponding angular momentum loss due to mass loss ( $\dot{J}_{\text{ML}}$ ) can be written as

$$\dot{J}_{\text{ML}} = \begin{cases} - \left( |\dot{M}_{\text{tr}}| - \beta \cdot \min(|\dot{M}_{\text{tr}}|, \dot{M}_{\text{Edd}}) \right) \left( \frac{M_{\text{d}}}{M_{\text{NS}} + M_{\text{d}}} \right)^2 a^2 \frac{2\pi}{P_{\text{orb}}}, & \dot{M}_{\text{tr}} \geq \dot{M}_{\text{cr}}, \\ - \left( |\dot{M}_{\text{tr}}| - \beta \cdot \min(|\dot{M}_{\text{tr}}|, \dot{M}_{\text{Edd}} \cdot d) \right) \left( \frac{M_{\text{d}}}{M_{\text{NS}} + M_{\text{d}}} \right)^2 a^2 \frac{2\pi}{P_{\text{orb}}}, & \dot{M}_{\text{tr}} < \dot{M}_{\text{cr}}, \end{cases} \quad (7)$$

where  $a$  is the binary separation.

### 3 RESULTS

#### 3.1 Observed Properties of AMXPs

In Table 1, we summarize some observed properties of 22 AMXPs collected from literature, including orbital period ( $P_{\text{orb}}$ ), spin period ( $P_s$ ), peak X-ray luminosity ( $L_X^{\text{peak}}$ ), donor mass ( $M_d$ ) and donor type. For most AMXPs, their donor masses are derived from binary mass functions by assuming  $M_{\text{NS}} = 1.4 M_{\odot}$  and the orbital inclination angle  $i = 75^\circ$  due to the lack of eclipses in their light curves. However, the donor masses of Aql X-1 and XSS J12270–4859 are obtained from their photometric data (Habets & Heintze 1981; de Martino et al. 2015). The peak X-ray luminosity ( $L_X^{\text{peak}}$ ) is estimated in terms of the observed maximum X-ray flux ( $F_X^{\text{max}}$ ) and the probable distance ( $D$ ), i.e.,  $L_X^{\text{peak}} = 4\pi D^2 F_X^{\text{max}}$ .

#### 3.2 Three Typical Evolutionary Tracks

To illustrate the characteristics of the evolution of CV-like, ultra-compact and diverging LMXBs, we present the evolution of key parameters of three typical binary systems in Figure 1.

For the system with an initial orbital period  $P_{\text{orb}}^i = 0.50$  d, the donor star is near the ZAMS when it starts mass transfer, and the system will evolve into a CV-like LMXB. It will experience two phases of mass transfer due to the effect of MB. At the first phase of mass transfer, the mass-transfer rate is larger than the critical mass-transfer rate, and the binary appears as a persistent source. When the donor star becomes fully convective, the binary soon becomes detached due to interrupted MB. As the binary separation decreases due to GR, the donor star will refill its Roche lobe. Therefore, there exists a period gap at an orbital period of 2–3 h. This system appears as a transient source at the second phase of mass transfer. At the final phase of mass transfer where the orbital period reverses, the donor star is a H-rich degenerate star, i.e., a brown dwarf.

For the system with  $P_{\text{orb}}^i = 2.50$  d, the donor star starts mass transfer near the terminal-age main sequence (TAMS) where the central hydrogen is almost exhausted. This system will ultimately evolve into a UCXB within 13.7 Gyr. In terms of the criterion of DIM, it will experience two phases as a persistent source and two phases as a transient source. After the RLOF starts, the mass-transfer rate increases rapidly and it appears as a persistent source within a remarkably short timescale ( $\sim 0.1$  Gyr). At the following phase, the mass-transfer rate declines and it appears as a transient LMXB for  $\sim 3$  Gyr until it evolves into

a UCXB. At the initial phase of UCXB, the mass transfer rate will increase until the minimum orbital period is approached. Then the donor star is fully degenerate. Because of the mass-radius relation of the He WD, the orbital period starts to increase and the mass-transfer rate declines all the time. When the mass-transfer rate is lower than the critical mass-transfer rate, the UCXB will become a transient source.

For the system with  $P_{\text{orb}}^i = 2.80$  d, the donor star starts mass transfer at the sub-giant branch and  $P_{\text{orb}}^{\text{RLOF}}$  is larger than  $P_{\text{orb}}^{\text{bif}}$ . The orbital period will increase and a diverging LMXB is formed. Meanwhile, the longer orbital period leads to a higher critical mass-transfer rate so that this system is almost always a transient source. When the RLOF terminates, the donor star ultimately becomes a He WD.

#### 3.3 $P_{\text{orb}} - M_d$ Plane

In Figure 2, we compare the evolutionary tracks of different LMXBs with the observed AMXPs in the  $P_{\text{orb}} - M_d$  plane. From this figure, we can see that the majority of AMXPs is located at the disk instability regions, except for the three AMXPs with BD donors, i.e., SAX J1808.4–3658, IGR J17379–3747 and IGR J00291+5934. Moreover, the two (quasi-)persistent X-ray sources, i.e., IGR J17602–6143 and MAXIJ0911–655, are likely located at the disk stability regions of UCXBs. This agreement between our results and observations implies that the DIM would be an important ingredient for understanding the formation of most AMXPs. In addition, the  $P_{\text{orb}} - M_d$  plane also provides a potential method to investigate the past and future evolution of an AMXP. These evolutionary tracks clearly show that the AMXPs with MS donors can evolve into AMXPs with extremely low-mass He WD donors. This indicates that there exists an evolutionary connection between them. In other words, these AMXPs with MS and extremely low-mass He WD donors could have the same origin, but are located at different evolutionary states. Particularly, Swift J1749.4–2807 is the only eclipsing AMXP, which implies that its donor mass is around  $0.63 M_{\odot}$  by assuming  $M_{\text{NS}} = 1.4 M_{\odot}$  and  $i = 75^\circ$ . In Figure 2, Swift J1749.4–2807 seems to be located near the disk stability region, thus we infer that it would be a persistent source not long ago. In addition, based on the position of Aql X-1 in Figure 2, we infer that it is likely formed from a diverging LMXB with  $P_{\text{orb}}^{\text{RLOF}}$  slightly larger than  $P_{\text{orb}}^{\text{bif}}$ . When the RLOF terminates, it will become a detached MSP+He WD binary with  $P_{\text{orb}} > 1$  d.

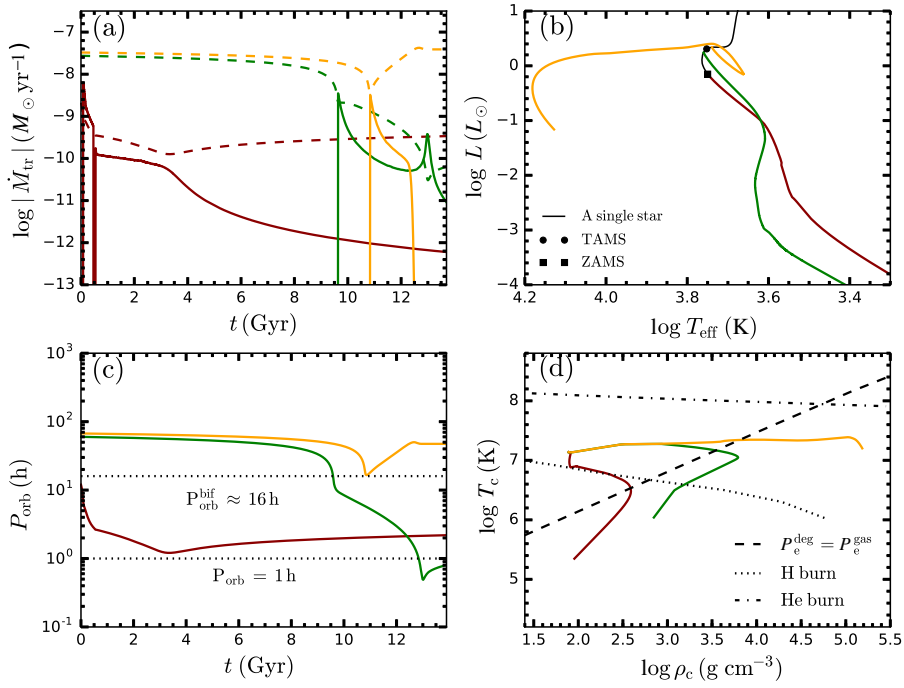


**Fig. 1** Evolution of key parameters for three typical binary systems with  $M_d^i = 1.0 M_\odot$  and different initial orbital periods, i.e.,  $P_{\text{orb}}^i = 0.50$  (dark red line), 2.50 (green line) and 2.80 d (orange line). Panel (a) shows the evolution of  $\dot{M}_{\text{tr}}$  (solid lines) and  $\dot{M}_{\text{cr}}$  (dashed lines) for the three binary systems as a function of time. Panel (b) presents the evolution of donor stars for the three binary systems (solid lines) and a single star with an initial mass of  $1.0 M_\odot$  from the ZAMS to the red giant branch (black solid line) in the HR diagram. Panel (c) shows the evolution of  $P_{\text{orb}}$  as a function of time for the three binary systems. The lower dotted line represents  $P_{\text{orb}} = 1$  h. Moreover,  $P_{\text{orb}}^{\text{bif}} \approx 16$  h (upper dotted line) for LMXBs with  $M_d^i = 1.0 M_\odot$  is also shown in panel (c). Panel (d) shows the evolution of donor stars for the three binary systems in the central temperature-central density ( $T_c - \rho_c$ ) plane. The dotted, dash-dotted and dashed lines in panel (d) represent the H burning line, the He burning line and the dividing line between degenerate matter and non-degenerate matter, respectively. Below the dividing line, the donor is a degenerate star.

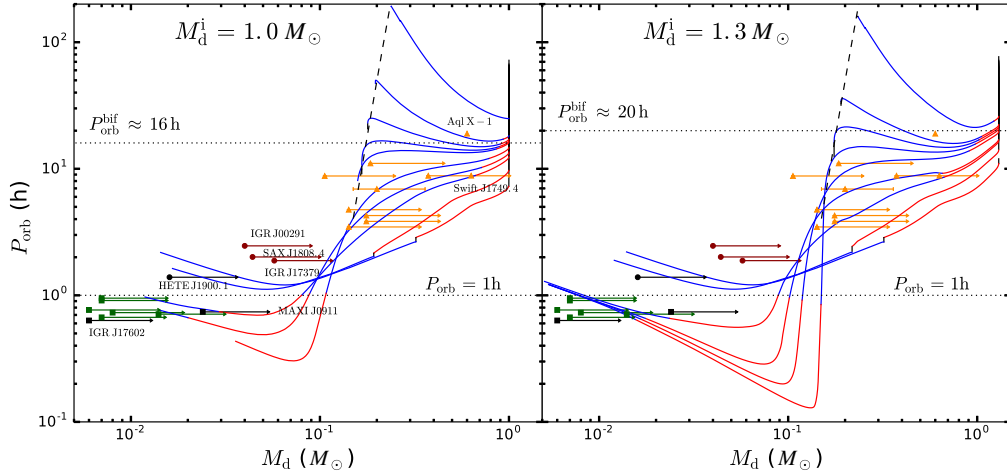


**Fig. 2** Evolutionary tracks of LMXBs with initial donor stars of  $1.0 M_\odot$  (left panel) and  $1.3 M_\odot$  (right panel) in the  $P_{\text{orb}} - M_d$  plane. The dashed line signifies the theoretical relation for detached binary millisecond pulsars with He WD companions (Lin et al. 2011). The red, blue and black solid lines in the evolutionary tracks are differentiated by  $\dot{M}_{\text{tr}} > \dot{M}_{\text{cr}}$ ,  $\dot{M}_{\text{tr}} < \dot{M}_{\text{cr}}$  and  $\dot{M}_{\text{tr}} < 10^{-13} M_\odot/\text{yr}$ , respectively. The different symbols indicate different donor types of AMXPs, including MS (solid triangles), BD (solid circles) and WD (solid squares). For most AMXPs, the ranges of their donor masses are inferred from binary mass functions by varying  $i$  from  $75^\circ$  to  $25.8^\circ$ . Besides, the three AMXPs marked with black color are (quasi-)persistent X-ray sources.

### 3.4 Transient and Persistent Behaviors

If the formation of most AMXPs is related to the DIM, our models may explain their transient and persistent behaviors. Usually, the time-averaged accretion rate<sup>1</sup> of the NS is assumed to be equal to the mass-transfer rate. Following Wijnands (2010), the time-averaged accretion rates of nine AMXPs lie between  $10^{-11} M_{\odot} \text{yr}^{-1}$  and  $10^{-9} M_{\odot} \text{yr}^{-1}$ . However, for the other AMXPs, it is difficult to estimate their time-averaged accretion rates due to the lack of time-averaged fluxes (Zhu et al. 2015). Based on the disk instability theory, the maximum accretion rate of the NS during a transient LMXB is  $\dot{M}_{\text{NS}}^{\text{max}} \simeq \min(|\dot{M}_{\text{tr}}|/d, \dot{M}_{\text{Edd}})$ . The value of  $\dot{M}_{\text{NS}}^{\text{max}}$  is obtained in terms of  $L_{\text{X}}^{\text{peak}} = GM_{\text{NS}}\dot{M}_{\text{NS}}^{\text{max}}/R_{\text{NS}}$ , where the NS radius ( $R_{\text{NS}}$ ) and  $M_{\text{NS}}$  are taken to be 10 km and  $1.4 M_{\odot}$ , respectively. Given that the duty cycles of typical transient X-ray sources are between 0.01 and 0.1, the maximum accretion rate of the NS is significantly larger than the mass-transfer rate and 10% or 1% of the observationally inferred maximum accretion rate will be close to the mass-transfer rate.

In Figure 3, we compare the mass-transfer rates of different LMXBs with the observationally inferred maximum accretion rates of AMXPs in the  $\log|\dot{M}_{\text{tr}}| - P_{\text{orb}}$  diagram. For most AMXPs with MS and WD donors, we can see that 10% or 1% of the maximum accretion rates of AMXPs are consistent with the mass-transfer rates of transient LMXBs from binary evolution calculations. Moreover, the two (quasi-)persistent X-ray sources, i.e., IGR J17602–6143 and MAXI J0911–655, seem to be located at different phases of persistent UCXBs. Namely, IGR J17602–6143 is located at the declining phase and MAXI J0911–655 is located at the increasing phase.

For CV-like LMXBs, their mass-transfer rates are always larger than the critical mass-transfer rate during the first mass-transfer phase. In other words, CV-like LMXBs always appear as a persistent source at this phase. Therefore, the AMXPs with MS donors can only be produced from LMXBs with  $P_{\text{orb}}^{\text{RLOF}}$  close to  $P_{\text{orb}}^{\text{bif}}$ , which can evolve into transient sources with low mass-transfer rates. The two transitional AMXPs, i.e., PSR J1023+0038 and XSS J12270–4859, have very faint X-ray luminosities of  $\sim 10^{34} \text{erg s}^{-1}$  corresponding to accretion rates of  $\sim 10^{-12} M_{\odot} \text{yr}^{-1}$ . Such an abnormal situation could be related to the sensitive dependence of accretion on the truncated position of the disk. When the inner radius of the disk is truncated near the co-rotation radius, the NS

can still accrete episodically due to the disc-field interaction, and then, it produces very faint X-ray luminosity (e.g., D’Angelo & Spruit 2010, 2012; Bozzo et al. 2018). For the three AMXPs with BD donors, i.e., SAX J1808.4–3658, IGR J17379–3747 and IGR J00291+5934, 1% of their maximum accretion rates are close to the mass-transfer rates of CV-like LMXBs. But all of them deviate from the evolutionary tracks of CV-like LMXBs in the  $P_{\text{orb}} - M_{\text{d}}$  plane. Particularly, the last AMXP with BD donor, HETE J1900.1–2455, is a quasi-persistent X-ray source with an X-ray luminosity of  $\sim 5 \times 10^{36} \text{erg s}^{-1}$ . The accretion rate of HETE J1900.1–2455 is estimated to be  $\sim 5 \times 10^{-10} M_{\odot} \text{yr}^{-1}$  and larger than the critical mass-transfer rate. Although we infer that HETE J1900.1–2455 is a persistent source, the location of HETE J1900.1–2455 in the  $P_{\text{orb}} - M_{\text{d}}$  plane indicates that it is more likely to be a transient source.

### 3.5 Donor Types

Due to the lack of the multi-wavelength observations of donors of most AMXPs, we cannot directly analyze the properties of donors from observations. Since AMXPs are in accretion states, the donor radii are approximately equal to the Roche lobe radii of donors ( $R_{\text{d,RL}}$ ). The value of  $R_{\text{d,RL}}$  can be given by Paczyński (1967),  $R_{\text{d,RL}} = (2GM_{\text{d}})^{1/3}(P_{\text{orb}}/9\pi)^{2/3}$ . It is widely assumed that if the  $R_{\text{d,RL}} - M_{\text{d}}$  relation for an AMXP with a measured orbital period intersects with the theoretical mass-radius relation of ZAMS stars, the donor star is roughly considered as an MS star (e.g., see fig. 3 in Krauss et al. 2005). Interestingly, the  $R_{\text{d,RL}} - M_{\text{d}}$  relations for the AMXPs with MS donors are located at the region between ZAMS and TAMS (see the dark orange lines in panel (a) of Fig. 4). If we use the  $R_{\text{d,RL}} - M_{\text{d}}$  relation to infer their donor types, we will find that their donors are mildly evolved. Therefore, whether this classification is reasonable or not should be checked carefully.

In panel (a) of Figure 4, we reanalyze their donor types with the evolutionary tracks of different LMXBs. Through the previous analysis, these AMXPs with MS donors are likely produced from LMXBs with  $P_{\text{orb}}^{\text{RLOF}}$  close to  $P_{\text{orb}}^{\text{bif}}$ , which can also evolve into transient LMXBs at the region between ZAMS and TAMS in the  $R_{\text{d}} - M_{\text{d}}$  plane. In panel (b) of Figure 4, it shows that the donor stars of LMXBs with  $P_{\text{orb}}^{\text{RLOF}}$  close to  $P_{\text{orb}}^{\text{bif}}$  have evolved and small helium cores<sup>2</sup> are formed in their interiors. If so, these

<sup>1</sup> The time-averaged accretion rate of the NS is estimated by adopting the time-averaged flux and assuming accretion onto a  $1.4 M_{\odot}$  NS with a 10 km radius (e.g., Bildsten & Chakrabarty 2001).

<sup>2</sup> In the MESA code, the boundary of the helium core is defined as the outermost location where the He abundance is less than 0.01.

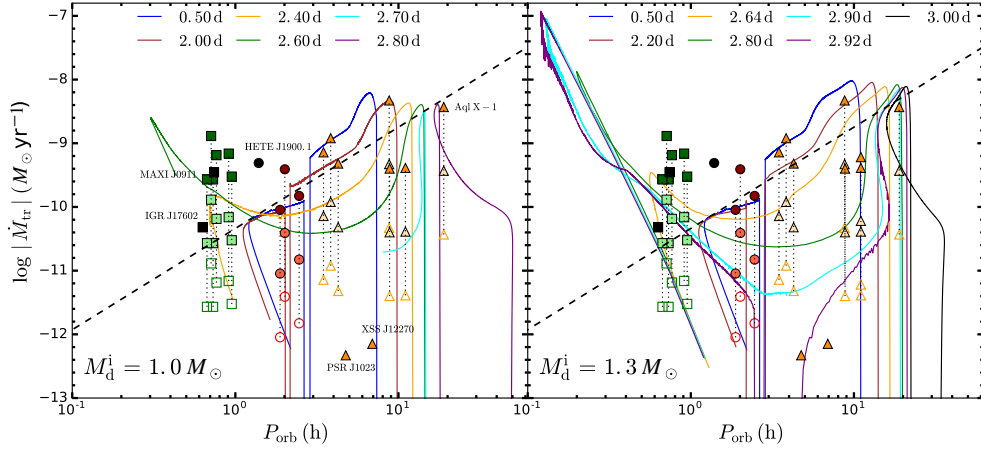


**Fig. 3** Evolutionary tracks of LMXBs with initial donor stars of  $1.0 M_{\odot}$  (left panel) and  $1.3 M_{\odot}$  (right panel) in the  $\log |\dot{M}_{\text{tr}}| - P_{\text{orb}}$  diagram. Different initial orbital periods are adopted to cover the evolution of CV-like, ultra-compact and diverging LMXBs. The *black dashed line* shows the value of  $\dot{M}_{\text{cr}}$  computed with Eq. (2). The *dark green squares*, *dark red circles* and *dark orange triangles* signify the maximum accretion rates of AMXPs with WD, BD and MS donors, respectively. The *light and open symbols* represent 10 and 1 per cent of the maximum accretion rates of AMXPs in transient LMXBs, respectively. Similar to Fig. 2, the *black symbols* represent the probable accretion rates of the three (quasi-)persistent X-ray sources.

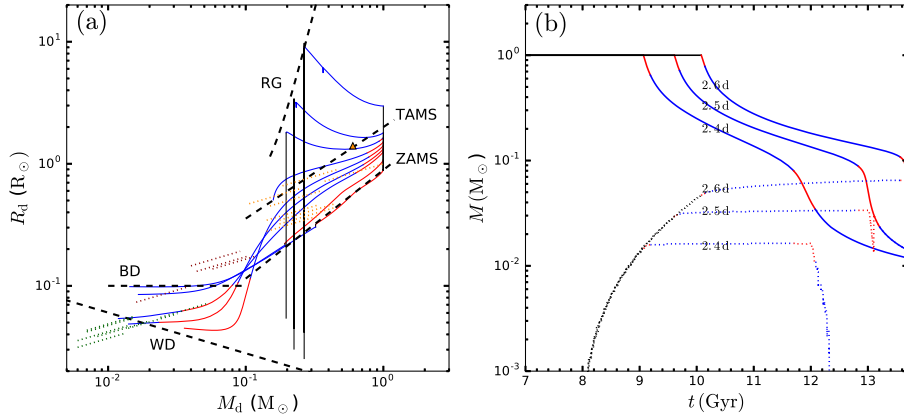


**Fig. 4** Donor radius as a function of donor mass for LMXBs with an initial donor star of  $1.0 M_{\odot}$  in panel (a). The *dashed lines* marked with “RG”, “TAMS”, “ZAMS”, “BD” and “WD” in panel (a) represent the theoretical mass-radius relations for red giants at their tips, TAMS stars, ZAMS stars, brown dwarfs and white dwarfs respectively (Demircan & Kahraman 1991; Sengar et al. 2017; Rappaport et al. 1995; Zdziarski et al. 2016). The *dotted lines with different colors* in panel (a) indicate that the probable ranges of the  $R_{\text{d, RL}} - M_{\text{d}}$  relations for AMXPs with different types of donors, i.e., MS (*dark orange*), BD (*dark red*) and WD (*dark green*), respectively. Similar to Fig. 2, the mass ranges of the donor stars of most AMXPs are determined by their maximum and minimum masses, which are derived from binary mass functions by assuming  $i = 25.8^{\circ}$  and  $75^{\circ}$ . The location of Aql X-1 is shown with a *triangle*. Panel (b) presents the evolution of the masses of donors (*solid lines*) and helium cores (*dotted lines*) for the three systems with  $P_{\text{orb}}^i = 2.4, 2.5, 2.6$  d, which can evolve into transient LMXBs at the region between ZAMS and TAMS in panel (a). In both panels (a) and (b), the *black, blue and red lines* represent  $\dot{M}_{\text{tr}} < 10^{-13} M_{\odot}/\text{yr}$ ,  $\dot{M}_{\text{tr}} < \dot{M}_{\text{cr}}$  and  $\dot{M}_{\text{tr}} > \dot{M}_{\text{cr}}$ , respectively.

AMXPs with MS donors are likely to have donor stars near the TAMS.

## 4 DISCUSSIONS

### 4.1 Influence of $\dot{M}_{\text{cr}}$

In our simulations, we assume that the accretion disk is always a solar-composition disk when we calculate the value of  $\dot{M}_{\text{cr}}$ . However, the chemical composition of the ac-

cretion disk depends on the surface abundance of the donor star, which should vary with initial binary parameters and time. In Panel (a) of Figure 5, we show the evolution of surface helium abundance ( $Y_{\text{s}}$ ) of donor stars as a function of orbital period for different types of LMXBs. For CV-like LMXBs, because the donor stars are relatively unevolved at the onset of RLOF, the surface abundance slightly deviates from the solar abundance so that the accretion disk can be treated as a solar-composition disk. But for UCXBs,

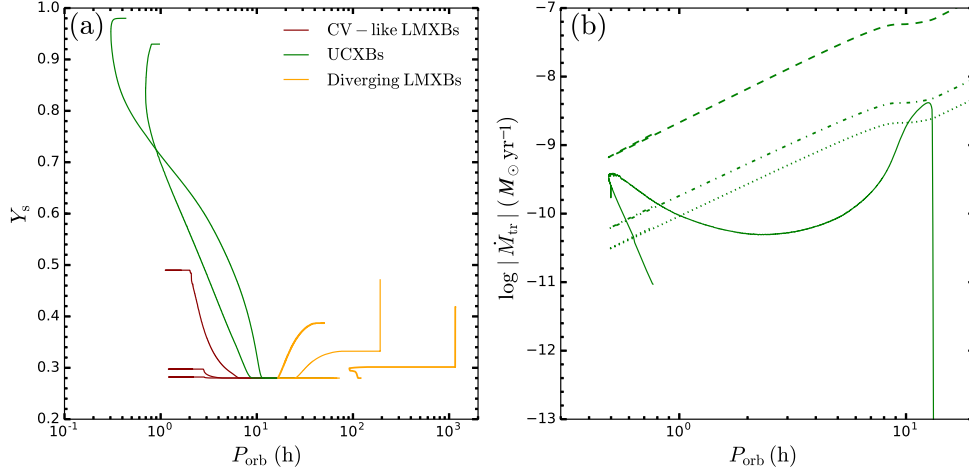


**Fig. 5** Surface helium abundance as a function of orbital period in panel (a). The initial binary parameters are  $M_d^i = 1.0 M_\odot$  and  $P_{\text{orb}}^i = 0.5, 1.0, 2.0, 2.5, 2.6, 2.8, 3.0, 3.5$  d. Similar to Fig. 1, the evolutionary tracks with different colors represent the evolution of different types of LMXBs. In panel (b), we present an example of the evolution of a UCXB (the *green solid line*) with  $M_d^i = 1.0 M_\odot$  and  $P_{\text{orb}}^i = 2.5$  d in the  $\log |\dot{M}_{\text{tr}}| - P_{\text{orb}}$  diagram. The *green dotted, dash-dotted and dashed lines* denote the corresponding critical mass-transfer rates under a solar-composition disk ( $X = 0.70, Y = 0.28, Z = 0.02$ ), a mixed-composition disk ( $X = 0.10, Y = 0.90$ ) and a pure-helium disk ( $Y = 1.0$ ), respectively (Lasota et al. 2008).

the donor stars have evolved at the beginning of RLOF and small helium cores are formed in their interiors. As the hydrogen envelopes of donor stars are stripped off, the surface helium abundance will notably change and the accretion disk should be a mixed-composition disk. Only when the donor stars become extremely low-mass He WDs, the transferred material is almost pure helium. For diverging LMXBs, the surface abundance does not strongly deviate from the solar abundance. In Panel (b) of Figure 5, we examine the effect of  $\dot{M}_{\text{cr}}$  on the evolution of a UCXB. From this figure, we can see that the dependence of  $\dot{M}_{\text{cr}}$  on the helium abundance is not significant for  $Y_s \leq 0.90$ . Since  $Y_s$  is less than 0.90 in most of the lives of UCXBs, our results will not be significantly influenced by this hypothesis.

## 4.2 Formation of Some Special AMXPs

Although our models can explain the properties of most AMXPs, it seems to be difficult to produce the four AMXPs with BD donors, especially in the  $P_{\text{orb}} - M_d$  plane. This indicates that some other mechanisms may play a role in the formation of these special AMXPs. In Figure 2, HETE J1900.1–2455 is located at the disk instability regions of CV-like LMXBs, but it appears as a quasi-persistent X-ray source in observation which shows a prolonged outburst duration of  $\sim 10$  yr (Degenaar et al. 2017). On the basis of the theoretical description of the DIM, the outburst duration is on the order of weeks to months (see equation (57) in Lasota 2001). The appearance of the quasi-persistent X-ray behavior could be de-

rived from the effect of irradiation, which can lead to a longer outburst duration compared to the effect of the DIM (e.g., Benvenuto et al. 2014; Lü et al. 2017). The other three AMXPs with BD donors, i.e., SAX J1808.4–3658, IGR J00291+5937 and IGR J17379–3747, are located at the same zones in the  $P_{\text{orb}} - M_d$  plane and all of them deviate from the evolutionary tracks of CV-like LMXBs. Moreover, an interesting phenomenon of SAX J1808.4–3658 is its anomalous orbital period derivative of  $\dot{P}_{\text{orb}} = (3.89 \pm 0.15) \times 10^{-12} \text{ s s}^{-1}$ , which is also incompatible with the theoretically inferred orbital period derivatives of typically CV-like LMXBs. Three possible mechanisms are proposed to explain this characteristic of SAX J1808.4–3658, i.e., the evaporation wind (Chen 2017), the tidal quadrupole interaction (Patruno et al. 2017) and the irradiation cycle (Tailo et al. 2018). In addition, SAX J1748.9–2021 also shows an orbital expansion with the orbital period derivative of  $\dot{P}_{\text{orb}} = (1.1 \pm 0.3) \times 10^{-10} \text{ s s}^{-1}$  (Sanna et al. 2016). However, Figure 2 shows that SAX J1748.9–2021 can evolve into a UCXB, and then its orbital period derivative should be negative during the MS phase. Such inconsistency might be related to the short-timescale observation, while our calculation is based on a long-timescale evolution.

## 5 SUMMARY AND CONCLUSIONS

Based on the binary evolutionary model of LMXBs and the model of accretion disk instability, we explore the formation and evolution of AMXPs. By comparing our results

with the observed properties of AMXPs, we obtain the following conclusions:

- (1) Most of the observed AMXPs are likely produced from LMXBs with orbital periods at the onset of Roche lobe overflow close to the bifurcation period. Meanwhile, the accretion disk instability may play an important role in the formation of most AMXPs.
- (2) The AMXPs with MS donors may ultimately evolve into AMXPs with extremely low-mass He WD donors. Particularly, the two (quasi-)persistent X-ray sources, i.e., MAXI J0911-655 and IGR J16597–3704, are likely explained by the increasing and declining phases of persistent UCXBs, respectively.
- (3) Regarding their donor types, our results indicate that these AMXPs with MS donors likely have donor stars near the TAMS.

**Acknowledgements** We thank the referee for his/her constructive suggestions, which helped us to improve the paper greatly. This work was supported by the National Natural Science Foundation of China (Nos. 11473063, 11522327, 11703081 and 11733008), Yunnan Foundation (Nos. 2015HB096 and 2017HC018), Youth Innovation Promotion Association of the Chinese Academy of Sciences (CAS), the CAS light of West China Program and CAS (No. KJZD-EW-M06-01).

## References

- Alpar, M. A., Cheng, A. F., Ruderman, M. A., & Shaham, J. 1982, *Nature*, 300, 728
- Altamirano, D., Wijnands, R., van der Klis, M., et al. 2010a, *The Astronomer’s Telegram*, 2565
- Altamirano, D., Patruno, A., Heinke, C. O., et al. 2010b, *ApJ*, 712, L58
- Archibald, A. M., Stairs, I. H., Ransom, S. M., et al. 2009, *Science*, 324, 1411
- Archibald, A. M., Bogdanov, S., Patruno, A., et al. 2015, *ApJ*, 807, 62
- Benvenuto, O. G., De Vito, M. A., & Horvath, J. E. 2014, *ApJ*, 786, L7
- Bildsten, L., & Chakrabarty, D. 2001, *ApJ*, 557, 292
- Bobrick, A., Davies, M. B., & Church, R. P. 2017, *MNRAS*, 467, 3556
- Bozzo, E., Ascenzi, S., Ducci, L., et al. 2018, *A&A*, 617, A126
- Bult, P. 2017, *ApJ*, 837, 61
- Campana, S., & Di Salvo, T. 2018, in *Astrophysics and Space Science Library*, 457, eds. L. Rezzolla, P. Pizzochero, D. I. Jones, N. Rea, & I. Vidana, 149 (arXiv:1804.03422)
- Casella, P., Altamirano, D., Patruno, A., Wijnands, R., & van der Klis, M. 2008, *ApJ*, 674, L41
- Chen, W.-C., & Panci, J. A. 2011, *A&A*, 527, A128
- Chen, H.-L., Chen, X., Tauris, T. M., & Han, Z. 2013, *ApJ*, 775, 27
- Chen, W.-C., & Podsiadlowski, P. 2016, *ApJ*, 830, 131
- Chen, W.-C. 2017, *MNRAS*, 464, 4673
- Coriat, M., Fender, R. P., & Dubus, G. 2012, *MNRAS*, 424, 1991
- Cumming, A., Zweibel, E., & Bildsten, L. 2001, *ApJ*, 557, 958
- D’Angelo, C. R., & Spruit, H. C. 2010, *MNRAS*, 406, 1208
- D’Angelo, C. R., & Spruit, H. C. 2012, *MNRAS*, 420, 416
- de Martino, D., Papitto, A., Belloni, T., et al. 2015, *MNRAS*, 454, 2190
- Degenaar, N., Ootes, L. S., Reynolds, M. T., Wijnands, R., & Page, D. 2017, *MNRAS*, 465, L10
- Deloye, C. J. 2008, in *American Institute of Physics Conference Series*, 983, 40 *Years of Pulsars: Millisecond Pulsars, Magnetars and More*, eds. C. Bassa, Z. Wang, A. Cumming, & V. M. Kaspi, 501
- Demircan, O., & Kahraman, G. 1991, *Ap&SS*, 181, 313
- Dubus, G., Lasota, J.-P., Hameury, J.-M., & Charles, P. 1999, *MNRAS*, 303, 139
- Falanga, M., Bonnet-Bidaud, J. M., Poutanen, J., et al. 2005, *A&A*, 436, 647
- Galloway, D. K., Chakrabarty, D., Morgan, E. H., & Remillard, R. A. 2002, *ApJ*, 576, L137
- Habets, G. M. H. J., & Heintze, J. R. W. 1981, *A&AS*, 46, 193
- Hartman, J. M., Patruno, A., Chakrabarty, D., et al. 2008, *ApJ*, 675, 1468
- Istrate, A. G., Tauris, T. M., & Langer, N. 2014, *A&A*, 571, A45
- Jia, K., & Li, X.-D. 2014, *ApJ*, 791, 127
- Jia, K., & Li, X.-D. 2015, *ApJ*, 814, 74
- Kaaret, P., Morgan, E. H., Vanderspek, R., & Tomsick, J. A. 2006, *ApJ*, 638, 963
- Krauss, M. I., Wang, Z., Dullighan, A., et al. 2005, *ApJ*, 627, 910
- Krimm, H. A., Markwardt, C. B., Deloye, C. J., et al. 2007, *ApJ*, 668, L147
- Landau, L. D., & Lifshitz, E. M. 1971, *The Classical Theory of Fields* (Oxford: Pergamon Press, 1971, 3rd rev. engl. edition)
- Lasota, J.-P. 2001, *New Astron. Rev.*, 45, 449
- Lasota, J.-P., Dubus, G., & Kruk, K. 2008, *A&A*, 486, 523
- Lin, J., Rappaport, S., Podsiadlowski, P., et al. 2011, *ApJ*, 732, 70
- Liu, W.-M., & Chen, W.-C. 2011, *MNRAS*, 416, 2285
- Lü, G., Zhu, C., Wang, Z., & Imminiyaz, H. 2017, *ApJ*, 847, 62
- Ma, B., & Li, X.-D. 2009, *ApJ*, 698, 1907
- Markwardt, C. B., Swank, J. H., Strohmayer, T. E., in ’t Zand, J. J. M., & Marshall, F. E. 2002, *ApJ*, 575, L21
- Markwardt, C. B., Swank, J. H., & Strohmayer, T. E. 2004, *The Astronomer’s Telegram*, 353
- Markwardt, C. B., Altamirano, D., Swank, J. H., et al. 2009, *The Astronomer’s Telegram*, 2197
- Nelson, L. A., & Rappaport, S. 2003, *ApJ*, 598, 431
- Paczyński, B. 1967, *Acta Astronomica*, 17, 287
- Papitto, A. 2016, *Mem. Soc. Astron. Italiana*, 87, 543
- Papitto, A., Bozzo, E., Ferrigno, C., et al. 2011, *A&A*, 535, L4

- Papitto, A., Ferrigno, C., Bozzo, E., et al. 2013, *Nature*, 501, 517
- Papitto, A., Torres, D. F., Rea, N., & Tauris, T. M. 2014, *A&A*, 566, A64
- Papitto, A., de Martino, D., Belloni, T. M., et al. 2015, *MNRAS*, 449, L26
- Patruno, A., Altamirano, D., Hessels, J. W. T., et al. 2009, *ApJ*, 690, 1856
- Patruno, A., & Watts, A. L. 2012, arXiv:1206.2727
- Patruno, A., Jaodand, A., Kuiper, L., et al. 2017, *ApJ*, 841, 98
- Paxton, B., Bildsten, L., Dotter, A., et al. 2011, *ApJS*, 192, 3
- Paxton, B., Cantiello, M., Arras, P., et al. 2013, *ApJS*, 208, 4
- Paxton, B., Marchant, P., Schwab, J., et al. 2015, *ApJS*, 220, 15
- Paxton, B., Schwab, J., Bauer, E. B., et al. 2018, *ApJS*, 234, 34
- Podsiadlowski, P., Rappaport, S., & Pfahl, E. D. 2002, *ApJ*, 565, 1107
- Poutanen, J., & Gierliński, M. 2003, *MNRAS*, 343, 1301
- Pylyser, E., & Savonije, G. J. 1988, *A&A*, 191, 57
- Pylyser, E. H. P., & Savonije, G. J. 1989, *A&A*, 208, 52
- Radhakrishnan, V., & Srinivasan, G. 1982, *Current Science*, 51, 1096
- Rappaport, S., Verbunt, F., & Joss, P. C. 1983, *ApJ*, 275, 713
- Rappaport, S., Podsiadlowski, P., Joss, P. C., Di Stefano, R., & Han, Z. 1995, *MNRAS*, 273, 731
- Rasio, F. A., Pfahl, E. D., & Rappaport, S. 2000, *ApJ*, 532, L47
- Ritter, H. 1988, *A&A*, 202, 93
- Roberts, M. S. E. 2013, in *IAU Symposium*, 291, Neutron Stars and Pulsars: Challenges and Opportunities after 80 years, ed. J. van Leeuwen, 127
- Ruderman, M. A., & Shaham, J. 1985, *ApJ*, 289, 244
- Sanna, A., Burderi, L., Riggio, A., et al. 2016, *MNRAS*, 459, 1340
- Sanna, A., Papitto, A., Burderi, L., et al. 2017, *A&A*, 598, A34
- Sanna, A., Bahramian, A., Bozzo, E., et al. 2018a, *A&A*, 610, L2
- Sanna, A., Ferrigno, C., Ray, P. S., et al. 2018b, *A&A*, 617, L8
- Sanna, A., Bozzo, E., Papitto, A., et al. 2018c, *A&A*, 616, L17
- Sengar, R., Tauris, T. M., Langer, N., & Istrate, A. G. 2017, *MNRAS*, 470, L6
- Shao, Y., & Li, X.-D. 2012, *ApJ*, 756, 85
- Shao, Y., & Li, X.-D. 2015, *ApJ*, 809, 99
- Strohmayer, T., & Keek, L. 2017, *ApJ*, 836, L23
- Strohmayer, T. E., Ray, P. S., Gendreau, K. C., et al. 2018, *The Astronomer's Telegram*, 11507
- Tailo, M., D'Antona, F., Burderi, L., et al. 2018, *MNRAS*, 479, 817
- Tauris, T. M., Sanyal, D., Yoon, S.-C., & Langer, N. 2013, *A&A*, 558, A39
- Tauris, T. M., & Savonije, G. J. 1999, *A&A*, 350, 928
- van Paradijs, J. 1996, *ApJ*, 464, L139
- Walter, R., & Ferrigno, C. 2017, *X-Ray Pulsars*, eds. A. W. Alsabti, & P. Murdin, *Handbook of Supernovae*, eds. A. W. Alsabti, & P. Murdin (Springer International Publishing AG), 1385
- Watts, A. L. 2012, *ARA&A*, 50, 609
- Wijnands, R., & van der Klis, M. 1998, *Nature*, 394, 344
- Wijnands, R., in't Zand, J. J. M., Rupen, M., et al. 2006, *A&A*, 449, 1117
- Williams, B. F., Naik, S., Garcia, M. R., & Callanan, P. J. 2006, *ApJ*, 643, 356
- Wijnands, R. 2010, *Highlights of Astronomy*, 15, 121
- Wu, Y. X., Yu, W., Li, T. P., Maccarone, T. J., & Li, X. D. 2010, *ApJ*, 718, 620
- Yan, Z., & Yu, W. 2015, *ApJ*, 805, 87
- Yungelson, L. R. 2008, *Astronomy Letters*, 34, 620
- Yungelson, L. R., Nelemans, G., & van den Heuvel, E. P. J. 2002, *A&A*, 388, 546
- Zdziarski, A. A., Ziółkowski, J., Bozzo, E., & Pjanka, P. 2016, *A&A*, 595, A52
- Zhu, C., Lü, G., & Wang, Z. 2015, *MNRAS*, 454, 1725